Food Chemistry: X 27 (2025) 102372

Contents lists available at ScienceDirect

Food Chemistry: X

journal homepage: www.sciencedirect.com/journal/food-chemistry-x

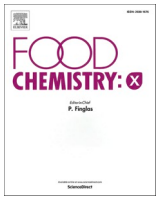

Soy protein isolate-chitosan complex condensate: Phase behavior, structure and functional properties

Xiongzhi Li [a,b], Chun Hu [a,b,*], Hailong Zhang [a,b], Lijuan Han [a,b], Weinong Zhang [a,b,*], Junbo He [a,b]

[a] Key Laboratory for Deep Processing of Major Grain and Oil, Ministry of Education, Hubei Key Laboratory for Processing and Transformation of Agricultural Products, Wuhan Polytechnic University, Wuhan 430023, China
[b] School of Food Science and Engineering, Wuhan Polytechnic University, Wuhan 430023, China

ARTICLE INFO

Keywords:
Soy protein isolate
Chitosan
Interaction mechanism
Spectroscopy
Structure
Functional properties

ABSTRACT

This study investigated the interaction mechanism between soy protein isolate (SPI) and chitosan (CS), and the structure and functional properties of their complex. The results revealed hydrogen bonding and hydrophobic interactions as the main driving forces for formation of soluble SPI/CS complex, while electrostatic interactions as the primary force driving insoluble complex formation. Insoluble complex formation was promoted by an appropriate increase in SPI/CS total concentration (> 0.24 %) and a decrease in NaCl concentration (< 60 mmol/L). After adding CS, SPI decreased in solubility, emulsifying and foaming properties, followed by an increase with pH raised from 3 to 9. CS addition could also change the tertiary structure of SPI and increase its relative crystallinity, enabling a red shift of amino ($-NH_2$) groups and a denser structure formation on SPI surface. These results offer valuable insights into the use of SPI/CS complex in the food industry.

1. Introduction

Protein and polysaccharide are widely present natural biological macromolecules, and they have been extensively applied in food, medicine and chemical fields due to their non-toxic, harmless and pollution-free properties (Benichou, Aserin and Garti, 2002). Recent studies have shown the great potential of protein and polysaccharide complexes in developing innovative foods with enhanced nutritional and functional properties (Gentile, 2020). These complexes can improve the texture, flavor and shelf life of food products, making them more appealing to consumers seeking healthier and more sustainable food (Gentile, 2020; Lu, Qian, Wu, Lan and Zhang, 2024). Proteins and polysaccharides primarily form complexes through two distinct mechanisms: (i) by establishing a stable structure via covalent bonding and (ii) by forming complex structures through non-covalent interactions, such as electrostatic forces, hydrophobic interactions and hydrogen bonds (Chobert, Gaudin, Dalgalarrondo and Haertlé, 2006). Protein and polysaccharide complexes not only can regulate the interface behavior of proteins by their interactions, but also affect their functional properties, such as foaming, emulsification and gelation (Zhang et al., 2019). For instance, chitosan, tremella fuciformis polysaccharide and acterial cellulose have been used to alter protein structure and enhance its solubility, emulsion stability and rheological properties (Wang, Li, Yan, Huang and Dong, 2016; Zhang et al., 2019). However, different protein and polysaccharide complexes vary in their functional properties due to the diverse and complex spatial structures of proteins.

Soy protein, the most important representative of legume protein, is highly similar to animal proteins in amino acid profile, leading to extensive use in the food industry (Yuan, Wan, Yang and Yin, 2014). Compared to animal proteins, soy protein is rich in essential amino acids and has the potential health benefits of preventing cardiovascular diseases, cerebrovascular diseases, and breast and prostate cancers (Qin, Wang and Luo, 2022). Additionally, soy protein is primarily composed of four distinct fractions: 2S, 7S, 11S and 15S, with low-molecular-weight globulin, cytochrome C, and trypsin inhibitors in the 2S fraction, while β-conglycinin, α-amylase and lipoxygenase in the 7S fraction, which can enhance the functional properties of soybean protein, such as emulsification, foaming, gelation and water absorption capabilities (Li et al., 2022 ; Zheng, Regenstein, Zhou and Wang, 2022). Despite these advantageous properties, soy protein also exhibits poor performance in

* Corresponding authors at: Key Laboratory for Deep Processing of Major Grain and Oil, Ministry of Education, Hubei Key Laboratory for Processing and Transformation of Agricultural Products, Wuhan Polytechnic University, Wuhan 430023, China.
E-mail address: huchun202020@163.com (C. Hu).

https://doi.org/10.1016/j.fochx.2025.102372
Received 31 October 2024; Received in revised form 9 March 2025; Accepted 10 March 2025
Available online 12 March 2025

solubility, water retention and emulsification in certain applications, such as acidic beverages, high-temperature cooking and dairy substitutes (Renkema and van Vliet, 2002).

Chitosan, a natural polysaccharide derived from chitin, exhibits good biocompatibility, biodegradability and superior mechanical properties (Xu, Tang, Yang, Wang and Zhou, 2020). This indicated that the combination of soy protein with chitosan can leverage their synergistic effects to enhance multiple functional properties. For instance, soy protein/chitosan complex has been reported to exhibit higher thermal stability and better gel-like properties than soy protein alone (Yuan, Wan, Yang and Yin, 2014). Additionally, the copolymers of soy protein with chitosan have been found to outperform soy protein alone in antioxidant properties (Wang, Li, Yan, Huang and Dong, 2016). However, the formation of soy protein/chitosan complexes is influenced by many factors, such as pH, ionic strength, temperature and solution ratio, because their variations can change the conditions of charge interactions and intermolecular forces, leading to different phase behaviors and ultimately affecting the structure and functional properties of complexes.

Therefore, this study aimed to comprehensively elucidate the interaction mechanism between soy protein isolate and chitosan at varying pH levels, as well as the effect mechanism of chitosan on the structure and functional properties of soy protein isolate. To this end, the impact of pH on the zeta-potential, particle size and turbidity of soy protein isolate/chitosan complex was measured, followed by analyzing the influence of chitosan on the structure and functional properties of soy protein isolate in terms of secondary, tertiary, crystalline structure and microstructure, as well as solubility, emulsifying and foaming properties. These findings will offer valuable theoretical insights into the application of soy protein isolate/chitosan complex in the food industry.

2. Materials and methods

2.1. Materials

Soybean meal (50 % protein) was supplied by Shandong Wonder Biotechnology Co., Ltd. (Shandong, China). Chitosan with an 80 %–90 % deacetylation degree (WM = 30,000), soybean oil, bicinchoninic acid (BCA), and bovine serum protein (BSA) was obtained from Shanghai Yuanye Biotechnology Co., LTD (Shanghai, China). Sodium hydroxide (NaOH), concentrated hydrochloric acid (HCl), sodium chloride (NaCl), sodium dodecyl sulfonate (SDS), 8-anilino-1-naphthalenesulfonic acid (ANS) and other analytical pure reagents were bought from Guoyao Chemical Reagent Co., Ltd. (Shanghai, China).

2.2. Extraction of soy protein isolate

Briefly, Soy protein isolate (SPI) was extracted as described by Zhang et al. (2020) with slight adjustments. Briefly, mildew-free and low-temperature-defatted soybean meal was crushed and sieved through an 80-mesh screen, following by mixing the soybean meal with water at a 1:15 mass ratio and stirring at pH 8.5 and 40 °C for 1 h to dissolve the protein. After centrifuging the mixture at 3000 rpm for 15 min to separate the slurry, the supernatant was adjusted to pH 4.5 (0.1 mol/L HCl), followed by another centrifugation at 3000 rpm for 15 min to collect the pellet. Finally, the precipitate was washed twice, dialyzed for 2 days and freeze-dried for further use.

2.3. Preparation of SPI/CS complex

Briefly, SPI (5 g) and CS (1 g) were separately dissolved in 500 mL of ultra-pure water and 100 mL of acetic acid buffer (0.6 %) and stirred for 4 h at room temperature (25 °C) to ensure complete hydration and dissolution. Next, the solutions were mixed at a specific mass proportion (SPI:CS = 5:1), and the complex pH was adjusted to desired levels with HCl (0.5, 1 and 6 mol/L) and NaOH (0.5, 1 and 4 mol/L) to minimize dilution.

2.4. Measurement of SPI/CS complex zeta-potential

The prepared sample was diluted to 0.1 mg/mL in aqueous solution with the same ionic strength but varying pH values. The zeta-potential was determined in triplicate by a Nano Zetasizer instrument (Malvern, UK) as described by He et al. (2024). The relative refractive index and absorptivity were set to 1.590 and 0.001, respectively, and the temperature was set at 25 °C with an equilibrium time of 1 min. Electrophoretic mobility (U_E) was used to calculate the zeta-potential (ζ) by eq. (1):

$$UE = \frac{2\varepsilon\zeta f(ka)}{3\eta}\# \quad (1)$$

where, U_E is the electrophoretic mobility ($m^2.v^{-1}.s^{-1}$); ε, the dielectric constant of solvent (F/m); f(ka), Henry constant; η, medium viscosity (Pa.s).

2.5. Determination of SPI/CS complex particle size

The nano laser particle size analyzer (Malvern Company, UK) was used to measure the particle size of SPI/CS complex under varying pH conditions as described by He et al. (2024). Briefly, the sample was prepared at a concentration of 0.1 mg/mL in water solutions with the same ionic strength but different pH values to avoid multiple light scattering. The relative refractive index and absorptivity were set to 1.590 and 0.001, respectively. Each sample was measured three times at 25 °C with a cycle of 10 times.

2.6. Measurement of SPI/CS complex solution turbidity

The turbidity of SPI/CS complex solution was measured at 600 nm using a multifunctional enzyme marker (Enspire, United States) under the conditions of different SPI/CS complex total concentrations (0.06 %, 0.12 %, 0.24 %, 0.48 % and 0.96 %), CS/SPI mass ratios (2,1, 1,1, 1:2, 1:5, 1:10 and 1:20), and salt ion concentrations (5, 10, 20, 40, 60 and 80 mM) (Niu et al., 2015). Each sample was placed in a quartz cuvette and measured three times in parallel at 25 °C. Turbidity (T) was calculated by eq. (2):

$$T = -\mathrm{In}\frac{I}{I_0}\# \quad (2)$$

where, I is the transmitted light intensity; I_0, the incident light intensity.

2.7. Determination of SPI solubility in SPI/CS complex system

Specifically, SPI and SPI/CS complex solutions at pH 3.0, 6.0 and 9.0 were diluted to 0.1 mg/mL using acetic acid buffers (0.3 %) with corresponding pH values, followed by centrifugation at 10000 rpm for 10 min to collect the supernatant. Next, the supernatant solution (1 mL) was placed in an enzyme-labeled plate, followed by adding 200 μL of BCA working fluid and standing for 20 min. Finally, each sample absorbance was measured in triplicate at 600 nm using a multifunctional enzyme marker (Enspire, United States) with BSA as a standard (Hu, Xiong, Xiong, Chen and Zhang, 2021).

2.8. Measurement of SPI/CS complex emulsifying properties

The emulsifying activity and stability of SPI/CS complex at pH 3.0, 6.0, and 9.0 were determined as reported by He et al. (2024) with slight adjustments. Briefly, each sample (3 mL) was combined with soybean oil (1 mL) in a beaker and homogenized at 10000 rpm for 1 min. At 0 and 10 min after homogenization, each 50 μL of the emulsion was mixed with SDS (0.1 %, 5 mL), followed by measuring the absorbance of each diluted emulsion at 500 nm. The emulsification activity index (EAI) and emulsification stability index (ESI) were determined using eq. (3) and

(4):

$$\mathrm{EAI}\ (\mathrm{m2/g}) = \frac{2 \times 2.303 \times A_0 \times 1000}{c \times \Phi \times 0.01 \times 10000}\# \quad (3)$$

$$\mathrm{ESI}\ (min) = \frac{A_0 \times 10}{A_0 - A_{10}}\# \quad (4)$$

where, A_0 is the absorbance at 0 min; C, protein weight per unit volume (g/mL); ϕ, oil volume fraction (0.25); A_{10}, 10 min absorbance.

2.9. Determination of SPI/CS complex foaming properties

The foaming capacity and stability of SPI/CS complex at pH 3.0, 6.0, and 9.0 were measured as reported by Wang, Li, Yan, Huang and Dong (2016) with minor modifications. Briefly, each 6 mL of SPI solution (5 mg/mL), SPI/CS complex solution (5 mg/mL SPI) and CS solution (5 mg/mL) were mixed separately with 24 mL of 0.3 % acetic acid buffer in a test tube. Then the samples were homogenized at 10000 rpm for 1 min. After shearing, the initial foam volume (V_0) and the foam volume 30 min later (V_{30}) were recorded. Finally, the foaming capacity (FC) and foaming stability (FS) were calculated using eq. (5) and (6), respectively:

$$\mathrm{FC\%} = \frac{V_0}{30} \times 100\# \quad (5)$$

$$\mathrm{FS\%} = \frac{V_{30}}{V_0} \times 100\# \quad (6)$$

2.10. Measurement of SPI/CS complex ultraviolet absorption spectra

The ultraviolet absorption spectra of SPI/CS complex at pH 3.0, 6.0 and 9.0 were determined in triplicate using an ultraviolet spectrophotometer (UV-6100, Yuanxi Instrument Corporation) according to the method described by He et al. (2024). Specifically, each sample was diluted to 0.25 mol/L with 0.3 % acetic acid buffer, followed by measurement in the wavelength range of 200 to 800 nm at a scanning interval of 0.5 nm.

2.11. Determination of SPI/CS complex fluorescence spectra

Briefly, the SPI/CS complex solutions at pH 3.0, 6.0 and 9.0 were separately diluted to 0.25 mol/L with 0.3 % acetic acid buffer, followed by measuring the endogenous fluorescence of each sample with a fluorescence spectrometer (Hitachi F-4600, Japan) using the method of Chao, Jung and Aluko (2018). The excitation wavelength was fixed at 295 nm, with a scanning range of 300 to 500 nm and a scan speed of 1200 nm/min. The slit widths were adjusted to 5 nm for both excitation and emission. Each sample was measured three times independently.

2.12. Measurement of SPI/CS complex surface hydrophobicity

The surface hydrophobicity of SPI/CS complex at pH 3.0, 6.0 and 9.0 was determined in triplicate following the method reported by Li, Wang, Zheng and Guo (2019), with slight modifications. Briefly, the SPI and SPI/CS complex with different pH values were diluted to different concentrations (0.1, 0.2, 0.5, 1 and 2 mg/mL) using 0.3 % acetic acid buffer and then each 20 μL ANS solution (pH 7.5) was added to each 4 mL sample solution, respectively. The excitation wavelength and emission wavelength were set at 390 nm and 470 nm, respectively. The surface hydrophobicity (Ho) was calculated from the initial slope of the fluorescence intensity curve of sample concentration.

2.13. Determination of SPI/CS complex Fourier transform infrared (FTIR) spectroscopy

The FTIR spectrum of SPI/CS complex was measured in triplicate using a Fourier infrared spectrometer (Nexus-670, USA) as described by Du et al. (2023). Briefly, the pH of SPI/CS complex solutions was adjusted to 3, 6 and 9, followed by freeze-drying for 48 h. Subsequently, each 2 mg sample was combined with potassium bromide (KBr) and ground into transparent flakes. Finally, the samples were scanned 64 times at a resolution of 4 cm^{-1} in the range of 4000–400 cm^{-1} to obtain their FTIR spectra.

2.14. Measurement of SPI/CS complex X-ray diffraction (XRD)

The crystal structures of SPI/CS complex were analyzed using an X-ray diffractometer (D8 ADVNCE, Germany) as reported by Du et al. (2023). Briefly, the pH of SPI/CS complex solutions was adjusted to 3, 6 and 9, followed by freeze-drying for 48 h and grinding each sample into powder. Finally, each sample was measured in triplicate at operating voltage and current of 40 kV and 30 mA, respectively. The diffraction angle (2θ) was scanned from 5° to 60° at 10°/min.

2.15. Microstructure of SPI/CS complex

The surface morphology of SPI/CS complex was observed using a scanning electron microscope (ZEISS-300, Germany) at 2 kV as described by Li et al. (2023), with slight adjustments. Specifically, the pH of SPI/CS complex solutions was adjusted to 3, 6 and 9, respectively, following by freeze-drying for 48 h. Finally, the freeze-dried sample was affixed to a copper conductive plate, sputter-coated with gold, and then photographed at 1000× magnification to obtain the SEM images.

2.16. Statistical analysis

Statistical analysis was conducted using SPSS software (Chicago, USA) with Duncan multiple comparison. Each experiment was independently replicated three times and the results were presented as mean ± standard deviation (SD, $n = 3$). Statistical significance was evaluated at a 5 % level.

3. Results and discussion

3.1. Effect of pH on zeta-potential and particle size of SPI/CS complex

Surface charge and particle size are of great importance for analyzing the dispersion and aggregation of colloidal particles (Hu and Xiong, 2022). Fig. 1A shows the effect of pH on the zeta-potential of SPI, CS and SPI/CS complex. When the pH increased from 1 to 12, the zeta-potential dropped from 10.87 to −8.35 mV and from 12.73 to −5.85 mV with a net charge of zero at pH 4.90 and pH 8.10 for SPI and CS, respectively, in contrast to a drop from 17.70 to −11.57 mV with a net charge of zero at pH 6.90 for SPI/CS complex. As shown above, after adding CS to SPI, the isoelectric point of SPI significantly shifted from 4.90 to 6.90, indicating that SPI and CS formed the SPI/CS complex through intermolecular interactions, resulting in a shift of the complex isoelectric point. Moreover, the zeta-potential of SPI/CS complex exhibited a trend similar to that of SPI alone, suggesting that SPI and CS were likely bound by hydrogen bonds, hydrophobic interactions and electrostatic interactions rather than chemical bonds (Hu and Xiong, 2022).

Fig. 1B presents the impact of pH on the average particle size of SPI, CS and SPI/CS complex. When pH shifted away from 4.90, the SPI mean particle size exhibited a decrease. A possible explanation is that when moving away from its isoelectric point, soy protein carried more charge which can increase mutual repulsion and enhance solubility, leading to the formation of smaller particles (Thrane, Paulsen, Orcutt and Krieger, 2017). At pH less than 8.10, CS exhibited a decrease in mean particle size, likely due to its increased solubility. After adding CS to SPI and at pH above or below 6.90, SPI in the complex system decreased in mean particle size, probably attributed to the reduced aggregation of SPI/CS complex when the pH value further moved away from the isoelectric

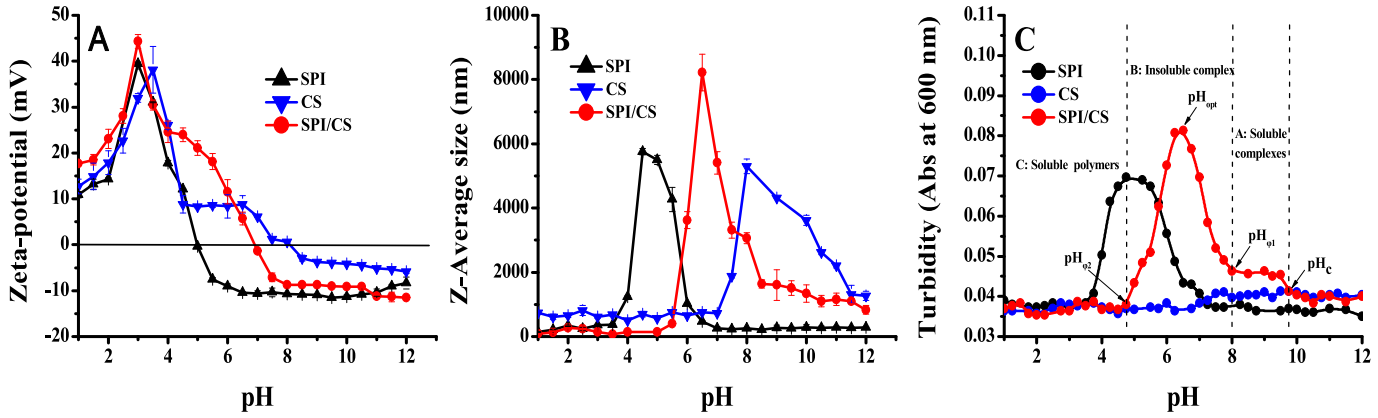

Fig. 1. The zeta-potential (A), mean particle size (B) and turbidity plot (C) of SPI, CS and SPI/CS complex under different pH conditions. SPI, soy protein isolate; CS, chitosan.

point (Niu et al., 2015).

3.2. Effect of pH on phase diagram of SPI/CS complex

The influences of pH on the turbidity of SPI, CS and SPI/CS complex are shown in Fig. 1C. The SPI/CS complex exhibited three different

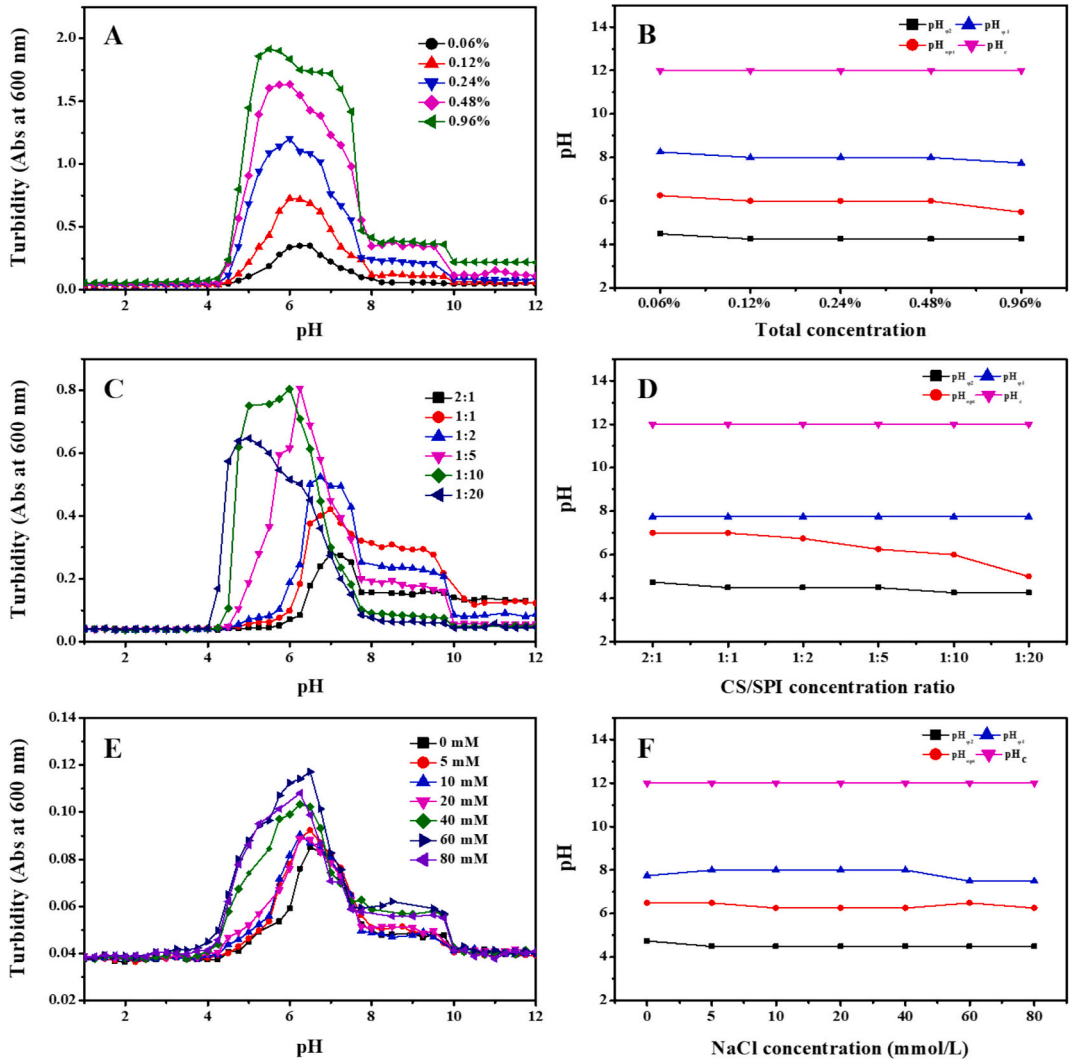

Fig. 2. Turbidity curves (A) and critical pH values (B) of SPI/CS complexes as a function of pH and total biopolymer concentration; Turbidity curves (C) and critical pH values (D) of SPI/CS complexes as a function of pH and CS/SPI concentration ratio; Turbidity curves (E) and critical pH values (F) of SPI/CS complexes as a function of pH and NaCl concentration. SPI, soy protein isolate; CS, chitosan.

phase regions: soluble complex formation region (8 < pH < 10) (A), insoluble complex formation region (4.5 < pH < 8) (B) and co-solution zone (pH < 4.5) (C). Additionally, the pH values of 9.75, 8.0, 6.5 and 4.75 corresponded to the initial point of soluble complex formation (pH_C), the initial point of insoluble complex formation ($pH_{\phi1}$), the peak point of insoluble complex formation (pH_{opt}), and the initial point of insoluble complex dissociation ($pH_{\phi2}$), respectively.

With pH increased from 1 to 3, SPI remained low and stable in turbidity, indicating its good solubility. With pH elevated from 3 to 7, its turbidity gradually increased to a peak and then decreased, suggesting the self-aggregation of SPI. With pH further raised from 7 to 12, the turbidity of SPI remained low and almost unchanged, indicating its good solubility and stability in alkaline conditions. Additionally, the CS turbidity remained almost constant with pH increased from 1 to 12. However, when CS was added to SPI, the soluble area of SPI showed an increase (pH < 4.5), accompanied by a decrease in its average particle size, suggesting the formation of a soluble complex between SPI and CS, possibly due to hydrogen bonding interactions between SPI and CS (Niu et al., 2015). Moreover, adding CS to SPI caused an increase in SPI turbidity value (4.5 < pH < 8), probably attributed to that at pH values above 4.90, SPI carried a negative charge while CS carried a positive charge, promoting the formation of electrostatic complexes. Furthermore, the mean particle size of SPI/CS complex increased significantly in this pH interval. Therefore, the formation of SPI/CS complex condensates can be inferred to be mainly driven by electrostatic attraction in this interval. At a pH value between 8 and 10, the SPI/CS complex turbidity exhibited a decrease, likely due to the formation of a soluble complex between SPI and CS (Niu et al., 2015). This was consistent with the observations of particle size and zeta-potential (Fig. 1A and B).

3.3. Effect of total concentration on the formation of SPI/CS complex

Fig. 2A and B show the influence of SPI/CS total concentration on the turbidity and key pH values (pH_C, $pH_{\phi1}$, pH_{opt} and $pH_{\phi2}$) during its formation. With the increase of its total concentration, the SPI/CS complex exhibited an increase in turbidity, likely due to the formation of larger molecular complex between SPI and CS (Niu, Su, Liu, Wang and Yang, 2014). Meanwhile, the phase zone of insoluble SPI/CS complex increased, in contrast to a decrease in the phase zone of soluble complex. This can be attributed to the increase of SPI/CS total concentration, which enhanced the frequency of effective intermolecular collisions and promoted the formation of condensed complexes between SPI and CS through electrostatic interactions (Hu, Xiong, Xiong, Chen and Zhang, 2021). In addition, with the increase of SPI/CS total concentration, the key pH values (pH_C and $pH_{\phi1}$) gradually shifted towards higher values. This can be due to the increase in the number of molecules and charge density in the system, which enhanced the frequency of effective intermolecular collisions, thereby promoting the formation of insoluble SPI/CS complex (Niu, Su, Liu, Wang and Yang, 2014). However, the $pH_{\phi2}$ exhibited a decrease, possibly attributable to the enhanced hydrogen bond interactions between SPI and CS with the decrease of system pH, facilitating the dissociation of insoluble condensates and the formation of soluble complexes.

3.4. Effect of SPI/CS concentration ratio on the formation of SPI/CS complex

The ratio of protein to polysaccharide is crucial for maintaining surface charge balance of biomacromolecules and facilitating complex agglomerate formation (Klein, Aserin, Ishai and Garti, 2010). Fig. 2C and D present the impact of CS/SPI concentration ratio on the turbidity and key pH values (pH_C, $pH_{\phi1}$, pH_{opt} and $pH_{\phi2}$) during SPI/CS complex formation. At the CS/SPI ratio below 1/5, the turbidity curve shifted to a lower pH, and the turbidity value increased, probably due to the dominance of excessive SPI in complex system properties, leading to SPI self-aggregation near its isoelectric point (pH 4.9). At the CS/SPI ratio of 1:5, the chitosan chain was fully saturated and adsorbed by SPI, resulting in maximum SPI/CS complex agglomeration. However, at the CS/SPI ratio above 1:5, the turbidity curve shifted to a higher pH value, and the complex condensate decreased with the increase of CS/SPI ratio, likely due to excessive CS coating on SPI surface, resulting in poor light scattering. Additionally, as CS/SPI ratio increased, the key pH values ($pH_{\phi2}$, pH_{opt} and $pH_{\phi1}$) decreased. A possible explanation for this decrease is that the protein molecules may not have sufficient negative charges to bind with chitosan to form a condensate, particularly in the presence of excessive chitosan, thus causing a shift towards a lower pH in the turbidity curve (Wang, Lee, Wang and Huang, 2007).

3.5. Effect of salt ion concentration on the formation of SPI/CS complex

Fig. 2E and F present the impact of sodium chloride (NaCl) concentration on the turbidity and key pH values (pH_C, $pH_{\phi1}$, pH_{opt} and $pH_{\phi2}$) during SPI/CS complex formation. At the salt ion concentration below 20 mM, the turbidity curves were similar without significant changes, suggesting a slight effect of low salt concentration on the formation of complex condensates. At the salt ion concentration between 20 mM and 60 mM, the turbidity curves increased obviously, resulting in a larger insoluble complex formation area and a smaller soluble complex formation area. This phenomenon was primarily induced by the interaction between small amounts of salt ions and biopolymers, which reduced inter- or intra-molecular repulsion, thereby increasing the solubility of proteins and polysaccharides (salt solubility effect) (Wang, Lee, Wang and Huang, 2007). However, at the salt ion concentration beyond 60 mM, the turbidity curve decreased, leading to a smaller insoluble complex formation area and a larger soluble complex formation area. One possible explanation is that at high salt ion concentrations, sodium and chloride ions competed with CS through adsorption onto the protein interface, thus reducing the number of CS molecules binding to SPI, leading to a decrease in turbidity (Ru, Wang, Lee, Ding and Huang, 2012). Another possible explanation is that at excessively high salt ion concentrations, the electrostatic interaction between SPI and CS was weakened due to electrostatic shielding effect (Xiong et al., 2016).

Additionally, as the salt ion concentration increased, the key pH values ($pH_{\phi1}$, pH_C and $pH_{\phi2}$) exhibited a down trend, possibly attributed to the electrostatic shielding effect of salt ions, leading to reduction in the surface charge of both SPI and CS. However, the pH decrease resulted in a positive charge increase in the system, thereby promoting the SPI/CS complex formation. With the increase of salt ion concentration, the pH_{opt} initially increased and then decreased, which was probably attributed to the increase of electrostatic shielding effect at higher salt ion concentrations, thus favoring the formation of complex agglomerates (Niu et al., 2015).

3.6. SPI solubility in SPI/CS complex solution

Fig. 3A presents the effect of pH on the solubility of SPI in the SPI/CS complex system. The solubility of SPI was higher at pH 3 and 9 than at pH 6, possibly because at pH 3 and 9, SPI molecules carried significant positive or negative charges, which increased electrostatic repulsion and reduced aggregation, thereby enhancing the solubility (O'Flynn, Hogan, Daly, O'Mahony, and Mccarthy, 2021). After adding CS to SPI at pH 3, the SPI solubility gradually increased, probably due to the formation of hydrogen bonds between SPI and CS, allowing more CS molecules to attach to the protein surface, thus enhancing the SPI hydrophilic properties (Hu, Xiong, Xiong, Chen and Zhang, 2021). However, when pH increased to 6, the SPI/CS complex system showed a significant drop in SPI solubility, likely attributed to.

electrostatic attraction, promoting the formation of a composite condensate between SPI and CS. With pH further increased to 9, the SPI solubility in the complex system increased, which was probably related to the weakening of electrostatic interaction between SPI and CS, leading to less precipitation and higher SPI solubility (Xue et al., 2018).

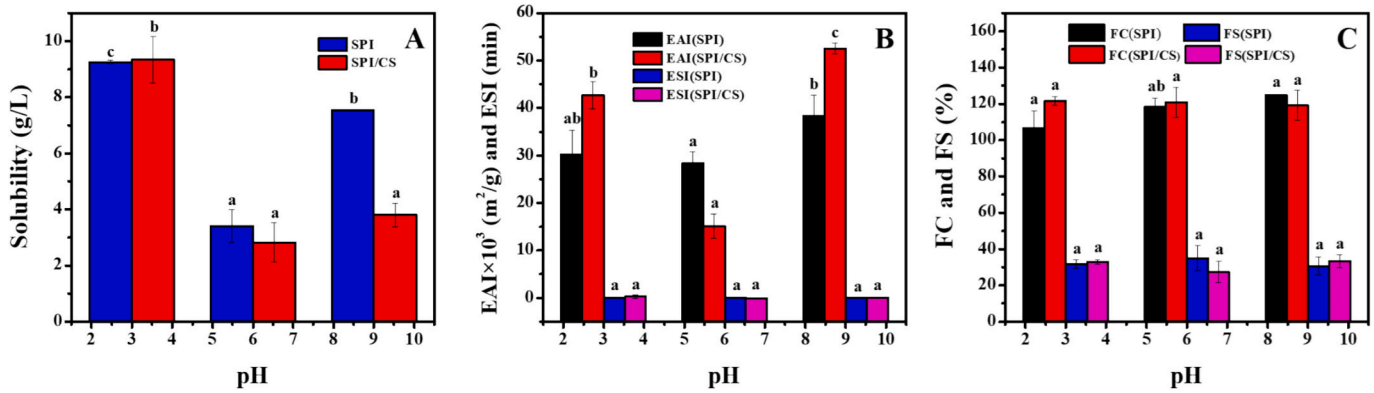

Fig. 3. The solubility (A) of SPI and SPI in the SPI/CS complex system as a function of pH (3, 6 and 9). Emulsifying properties (B) and foaming properties (C) of SPI and SPI/CS complex as a function of pH (3, 6 and 9). SPI, soy protein isolate; CS, chitosan; EAI, emulsifying activity index; ESI, emulsifying stability index; FC, foaming capability; FS, foaming stability. Different small letters over the bars indicate significant difference between different samples at $p < 0.05$.

3.7. Emulsifying and foaming properties of SPI/CS complex

The impact of pH on the emulsifying properties of SPI/CS complex is presented in Fig. 3B. With pH increased from 3 to 6, no significant change was observed in the emulsifying activity index (EAI) of SPI. However, as pH increased to 9, SPI increased.

in EAI, probably related to its increased solubility. After adding CS to SPI at pH 3, the EAI of SPI/CS complex increased, likely due to the interaction between SPI and CS, enhancing its adsorption capacity at the oil/water interface (Kumar, Ganesan, Selvaraj and Rao, 2014). When pH increased from 3 to 6, the EAI of SPI/CS complex decreased significantly, which was likely due to the formation of insoluble SPI/CS complex induced by electrostatic interaction, thereby reducing protein adsorption at the interface (He et al., 2024). However, when pH increased to 9, the SPI/CS complex increased in EAI, likely due to the higher solubility of SPI.

Additionally, as shown in Fig. 3B, with the increase of pH from 3 to 6, the emulsifying stability index (ESI) of SPI decreased, likely due to the reduction of surface hydrophobicity, weakening the conformation flexibility of SPI (Saricaoglu, 2019). When pH further increased to 9, the ESI of SPI increased, probably related to the increase of protein solubility and charge density. After adding CS to SPI at pH 3, the ESI of SPI/CS complex increased, likely because CS addition could balance the hydrophilicity and hydrophobicity of SPI. However, when pH increased from 3 to 9, the ESI decreased significantly in the SPI/CS complex system, likely attributed to the formation of electrostatic complexes between SPI and CS.

Fig. 3C presents the influence of pH on the foaming properties of SPI and SPI/CS complex. When pH increased from 3 to 9, SPI gradually improved in foaming capability (FC) and stability (FS), which was probably contributed by its enhanced solubility, reducing its average particle size and enabling its rapid adsorption on the air/water interface to form a stable interfacial film (Yuan, Ren, Zhao, Luo and Gu, 2012). After adding CS to SPI at pH 3, the FC and FS of SPI in the complex system showed an uptrend, which can be attributed to hydrogen bond interactions between CS and SPI, exposing hydrophilic amino acids or groups on the SPI surface, and enabling a more homogeneous dispersion of SPI in the solution. However, when pH increased from 3 to 6, the SPI/CS complex system decreased in FC and FS, probably due to electrostatic interactions between SPI and CS, leading to a large amount of precipitation (Liu, Zhong, Liu, Tu and Wan, 2011). When pH increased from 6 to 9, the SPI/CS complex remained almost unchanged in FC, but improved in FS. This improvement in stability might be attributed to the weakening electrostatic interactions between SPI and CS, reducing aggregation and forming a more stable interfacial film (Li et al., 2017).

3.8. Ultraviolet (UV) and fluorescence spectra of SPI/CS complex

Ultraviolet-visible (UV–Vis) light absorption is a very simple and effective method for exploring the changes of protein tertiary structure (Li et al., 2017). Fig. 4A presents the impact of pH on UV absorption spectra of SPI, CS and SPI/CS complex. With pH increased from 3 to 6, SPI showed an increase in maximum UV absorption intensity at 265 nm, probably related to the exposure of some aromatic amino acid residues to the solution. As pH further increased from 6 to 9, SPI decreased in the maximum UV absorption intensity, likely due to the sensitivity of tyrosine and tryptophan to the alkaline conditions, leading to the burial of these residues (Hu and Xiong, 2022). Moreover, the position of its maximum UV absorption peak at 265 nm did not change significantly at varying pH values, suggesting that the fundamental structure of SPI was not significantly affected by these pH changes.

Additionally, CS exhibited no UV absorption peak under different pH conditions. However, when CS was added to SPI at pH 3, SPI decreased in maximum UV absorption peak intensity, likely due to CS covering the SPI surface and shielding the tyrosine and tryptophan residues (Hu and Xiong, 2022). When pH increased from 3 to 6, SPI exhibited an increase in maximum UV absorption peak intensity in the complex system, likely attributable to the formation of electrostatic complexes between SPI and CS (He et al., 2024). With pH further increased to 9, SPI decreased in the maximum absorption peak intensity of the complex system, which might be induced by the formation of electrostatic interactions between SPI and CS, causing CS to bind to the protein surface, thereby shielding the tyrosine and tryptophan residues. In the complex system, SPI showed no significant change in maximum absorption peak position, suggesting that the structure of SPI dissolved in the complex system remained almost unchanged.

The UV–Vis results were further verified by using fluorescence spectroscopy to detect protein conformational changes in the complex system (He et al., 2024). Fig. 4B presents the influence of pH on the fluorescence spectra of SPI, CS and SPI/CS complex. When pH increased from 3 to 9, SPI increased in maximum fluorescence emission peak intensity, which might be attributed to changes in protein solubility. Meanwhile, the maximum fluorescence emission peak position of SPI shifted from 331 nm to 333 nm with increasing pH, suggesting that pH could change the micro-environment of SPI.

As shown in Fig. 4B, CS exhibited a small fluorescence emission peak that was unaffected by pH variations. However, after adding CS to SPI at pH 3, the SPI/CS complex increased in maximum fluorescence emission peak intensity, likely due to the binding of CS to SPI surface, and thus encapsulating the tryptophan residues (Shi et al., 2019), which was consistent with the results of UV spectroscopy (Fig. 4A). As pH increased from 3 to 6, the SPI/CS complex increased in maximum fluorescence emission peak intensity and this increase might be associated with

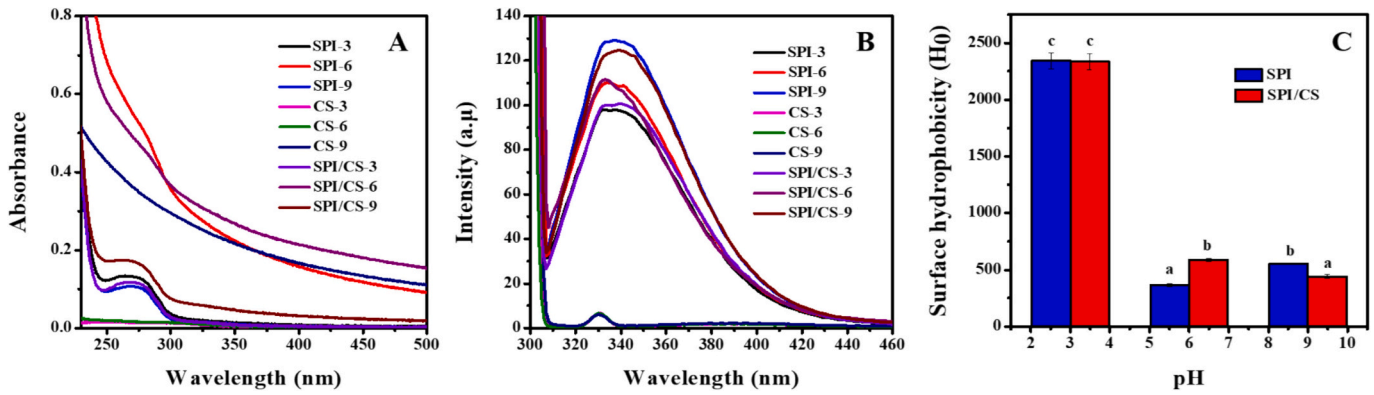

Fig. 4. The ultraviolet spectrum (A), fluorescence spectrum (B) and surface hydrophobicity (C) of SPI, CS and SPI/CS complex as a function of pH (3, 6 and 9). SPI, soy protein isolate; CS, chitosan. Different small letters over the bars indicate significant difference between different samples at $p < 0.05$.

electrostatic interactions between SPI and CS, leading to conformational changes in SPI. With pH further increased to 9, the SPI/CS complex showed a further increase in maximum fluorescence emission peak intensity, suggesting a deeper embedding of tryptophan residues, probably because CS became nearly insoluble and covered the SPI surface at pH 9. Additionally, after adding CS to SPI at pH 3, the SPI/CS complex shifted from 331 nm to 333 nm in the position of maximum fluorescence emission peak, and this position further shifted from 333 nm to 339 nm with pH increased from 3 to 9. These results suggested that CS addition and pH induction can cause greater exposure of tyrosine and tryptophan residues to a hydrophilic environment.

3.9. Surface hydrophobicity of SPI/CS complex

Fig. 4C shows the impact of pH on the surface hydrophobicity of SPI and SPI/CS complex. With the increase of pH from 3 to 6, SPI significantly decreased in surface hydrophobicity. This could be explained by the ionization of amino and carboxyl groups in SPI at a high pH value, which enhanced their interaction with water (Li, Kang, Zou, Xu and Zhou, 2015). When pH further increased to 9, its surface hydrophobicity increased. This increase might be induced by changes in partial charges of SPI under alkaline conditions, loosening its structure and exposing internal hydrophobic regions, thereby increasing its surface hydrophobicity. Additionally, after adding CS to SPI at pH 3, SPI decreased in the surface hydrophobicity, probably due to complex formation between CS and SPI.

altering the protein structure or molecular interactions, leading to the masking or redistribution of hydrophobic regions (Zhang et al., 2015). Moreover, as pH increased from 3 to 9, the SPI/CS complex decreased in surface hydrophobicity, which was likely contributed by deprotonation of protein carboxyl groups, increasing negative charge and solubility, thereby reducing the exposure of hydrophobic groups (Bing, Li, Sun, Wang and Liang, 2023).

3.10. Fourier transform infrared spectroscopy of SPI/CS complex

Fig. 5A shows the influence of pH on the FTIR spectra of freeze-dried SPI, CS and SPI/CS complex. SPI showed characteristic absorption peaks of amino acids at 3299.30 cm^{-1} at pH 3, which were mainly attributed to the stretching vibration of amino (-NH_2) groups. The amide I band at 1648.03 cm^{-1}, was mainly assigned to the stretching vibration of C═O bonds; the amide II band at 1535.61 cm^{-1}, was related to NH- stretching vibration; the amide III band around 1230.99 cm^{-1}, was mainly ascribed to C—N and N—H stretching vibrations (Hu and Xiong, 2022). As pH increased from 3 to 9, SPI exhibited little variation in FTIR spectra, suggesting that pH had little effect on SPI structure. However, the characteristic absorption peak of amino acids shifted from 3299.83 cm^{-1} to 3292.60 cm^{-1}, possibly due to the exposure of amino acids to a

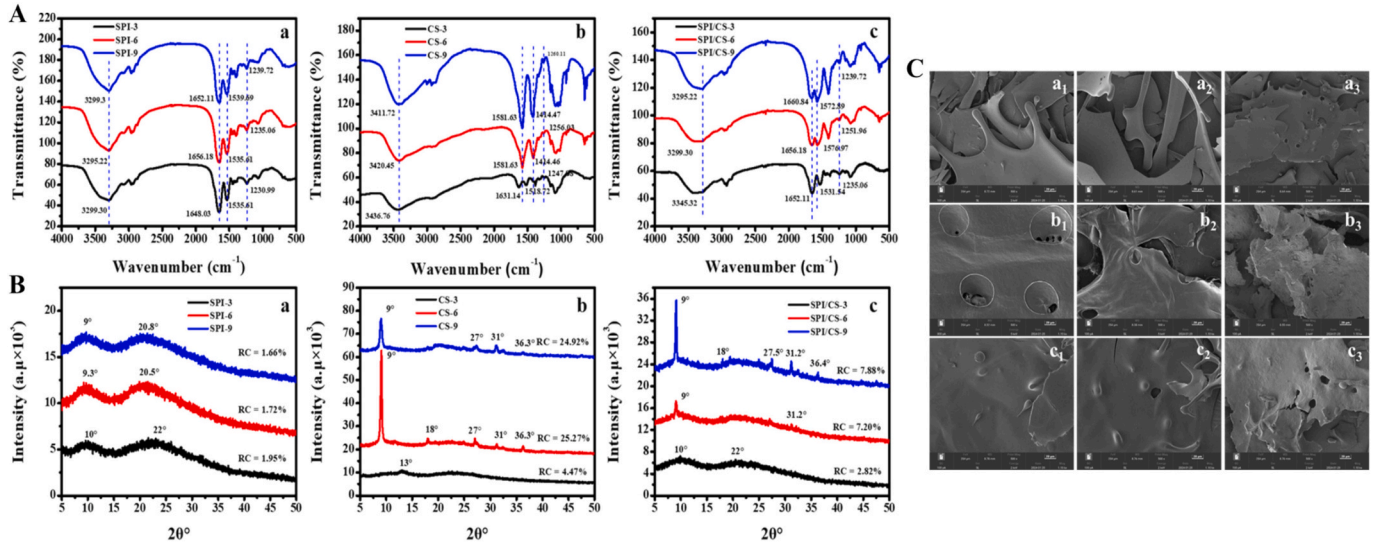

Fig. 5. The infrared spectrum (A) and X-ray diffraction pattern (B) of SPI, CS and SPI/CS complex as a function of pH (3, 6 and 9). Microstructure images (C) of SPI (a_1 (pH = 3), a_2 (pH = 6) and a_3 (pH = 9)), CS (b_1 (pH = 3), b_2 (pH = 6) and b_3 (pH = 9)), and SPI/CS complex (c_1 (pH = 3), c_2 (pH = 6) and c_3 (pH = 9)) as a function of pH. SPI, soy protein isolate; CS, chitosan.

more hydrophobic environment.

At pH 3, CS exhibited amino characteristic absorption peak at 3436.76 cm^{-1}, C—O stretching vibration peak at 1631.14 cm^{-1} and -NH angular degeneration peak at 1518.72 cm^{-1} (Fig. 5Ab) (Ding, Nie, Deng, Xiao and Shi, 2013). Moreover, as pH increased from 3 to 9, CS remained almost consistent in the types of peaks observed, indicating that pH had no obvious effect on CS structure. However, with increasing pH, the amino characteristic absorption peak exhibited a blue shift, probably due to the exposure of CS amino to a more hydrophobic environment.

After adding CS to SPI at pH 3, the SPI/CS complex exhibited a FTIR spectrum similar to that of SPI alone, indicating that no chemical reaction occurred between them. However, the amino stretching vibration peak of SPI shifted from 3345.32 cm^{-1} to 3295.22 cm^{-1}, suggesting the occurrence of interaction between SPI and CS. Furthermore, the blue shift was more obvious with pH increased from 3 to 9, implying enhanced interaction between SPI and CS.

3.11. X-ray diffraction of SPI/CS complex

The impact of pH on X-ray diffraction patterns of SPI, CS and SPI/CS complex is presented in Fig. 5B. In Fig. 5Ba, it is shown that at pH 3, SPI exhibited a relative crystallinity of 1.95 % with two distinct crystallization peaks at 10° and 22°, respectively (Waglay, Achouri, Karboune, Zareifard and L'Hocine, 2019). With the increase of pH from 3 to 9, no significant changes were observed in the relative crystallinity or the positions of crystallization peaks of SPI, suggesting that pH had little effect on its relative crystallinity.

Additionally, at pH 3, CS exhibited a single prominent crystallization peak at 13° with a relative crystallinity of 4.47 %. When pH increased to 6 and 9, the number of crystallization peaks increased, and the relative crystallinity rose from 4.47 % to 25.27 % and 24.92 %, respectively. This was likely attributed to the exposure of crystallization peaks in CS induced by the pH change, leading to a higher relative crystallinity (He et al., 2024).

After adding CS to SPI, SPI exhibited two crystallization peaks at 10° and 22°, with no significant change in its relative crystallinity. However, with pH increased to 6, the number of crystallization peaks and the relative crystallinity increased, possibly due to the formation of an electrostatic complex between SPI and CS. With pH further increased to 9, the SPI/CS complex exhibited a noticeable change in the number of crystal peaks, and the relative crystallinity increased to 7.88 %. This could be contributed by the formation of SPI/CS soluble complexes, leading to the simultaneous appearance of SPI and CS crystallization peaks.

3.12. Microstructure of SPI/CS complex

Fig. 5C shows the microstructure of freeze-dried SPI, CS and SPI/CS complex under different pH conditions. As pH increased from 3 to 9 (Fig. $5Ca_1$-a_3), SPI exhibited a consistently smooth surface, indicating that the pH had no significant effect on its surface structure. At pH 3, the CS surface also appeared smooth (Fig. $5Cb_1$), but it exhibited a rough membrane structure at pH 6 and 9 (Fig. $5Cb_2$ and b_3), probably due to CS aggregation under these pH conditions. After CS addition at pH 3 (Fig. $5Cc_1$), the SPI/CS complex exhibited a rough surface, which was likely induced by the attachment of CS to the SPI surface. With pH increased to 6 (Fig. $5Cc_2$), the SPI/CS complex formed a rougher structure, probably attributed to electrostatic interactions between SPI and CS molecules and CS film-forming properties (Wang, Li, Yan, Huang and Dong, 2016). When pH further increased to 9 (Fig. $5Cc_3$), the SPI/CS complex exhibited a coarser surface, probably due to CS film-forming properties.

4. Conclusion

This study elucidated the interaction mechanism between SPI and CS, as well as the influence of CS on SPI structure and functional properties. Hydrogen bonding and hydrophobic interactions were shown to drive soluble SPI/CS complex formation, while electrostatic interactions were crucial for insoluble SPI/CS complex formation. An appropriate increase in SPI/CS complex concentration (> 0.24 %) and a reduction in NaCl concentration (< 60 mmol/L) were found to favor insoluble SPI/CS complex formation. Additionally, after CS addition, SPI exhibited a decrease in solubility, emulsifying and foaming properties, followed by an increase with pH elevated from 3 to 9. Moreover, CS addition can reduce SPI surface hydrophobicity, increase its relative crystallinity, and induce a red shift in SPI amino ($-NH_2$) groups. Furthermore, CS addition contributed to the formation of a denser structure on the SPI surface. These findings provide theoretical insights into the application of SPI/CS complexes in food formulations.

CRediT authorship contribution statement

Xiongzhi Li: Writing – original draft, Methodology, Data curation. **Chun Hu:** Writing – review & editing, Writing – original draft, Supervision, Project administration, Funding acquisition. **Hailong Zhang:** Formal analysis, Conceptualization. **Lijuan Han:** Supervision, Software, Resources. **Weinong Zhang:** Resources, Project administration, Methodology. **Junbo He:** Visualization, Validation.

Declaration of competing interest

The authors declare that they have no known competing financial interests or personal relationships that could have appeared to influence the work reported in this paper.

Acknowledgements

This work was financially supported by Research Funding of Wuhan Polytechnic University (2024RZ067), the Open Project of the Key Laboratory of Major Grain and Oil Deep Processing Ministry of Education (DZLY2022002), and National Natural Science Foundation project of China (32072134).

Data availability

The data that has been used is confidential.

References

Benichou, A., Aserin, A., & Garti, N. (2002). Protein-polysaccharide interactions for stabilization of food emulsions [review]. *Journal of Dispersion Science and Technology, 23*(1–3), 93–123.

Bing, S., Li, Y., Sun, G., Wang, C., & Liang, Y. (2023). Effect of different acidic or alkaline environments on structural characteristics, functional and physicochemical properties of lentinus edodes protein. *Process Biochemistry, 130*, 15–25.

Chao, D., Jung, S., & Aluko, R. E. (2018). Physicochemical and functional properties of high pressure-treated isolated pea protein. *Elsevier, 45*, 178–185.

Chobert, J. M., Gaudin, J. C., Dalgalarrondo, M., & Haertlé, T. (2006). Impact of Maillard type glycation on properties of beta-lactoglobulin. *Biotechnology Advances, 24*(6), 629–632.

Ding, F., Nie, Z., Deng, H., Xiao, L., & Shi, X. (2013). Antibacterial hydrogel coating by electrophoretic co-deposition of chitosan/alkynyl chitosan. *Carbohydrate Polymers, 98*(2), 1547–1552.

Du, M., Chen, L., Din, Z.-u., Zhan, F., Chen, X., Wang, Y., … Ding, W. (2023). Structure and surface properties of ozone-conjugated octenyl succinic anhydride modified waxy rice starch: Towards high-stable Pickering emulsion. *International Journal of Biological Macromolecules, 253*(3), Article 126895.

Gentile, L. (2020). Protein-polysaccharide interactions and aggregates in food formulations. *Current Opinion in Colloid & Interface Science, 48*, 18–27.

He, Y., Hu, C., Zhang, W., He, J., Chen, L., Lijuan, H., & Cong, Y. (2024). Modulation of rapeseed protein nanoparticles by interaction with chitosan: Enhancing the physical stability, antioxidant activity and β-carotene slow-release properties of Pickering emulsion. *Industrial Crops and Products, 221*, Article 119341.

Hu, C., & Xiong, H. (2022). Structure, interfacial adsorption and emulsifying properties of potato protein isolate modified by chitosan. *Colloids and Surfaces A: Physicochemical and Engineering Aspects, 638*, Article 128314.

Hu, C., Xiong, Z., Xiong, H., Chen, L., & Zhang, Z. (2021). Effects of dynamic high-pressure microfluidization treatment on the functional and structural properties of potato protein isolate and its complex with chitosan. *Food Research International, 140* (1), Article 109868.

Klein, M., Aserin, A., Ishai, P. B., & Garti, N. (2010). Interactions between whey protein isolate and gum Arabic. *Colloids and Surfaces. B, Biointerfaces, 79*(2), 377–383.

Kumar, K. S., Ganesan, K., Selvaraj, K., & Rao, P. V. S. (2014). Studies on the functional properties of protein concentrate of Kappaphycus alvarezii (Doty) Doty-an edible seaweed. *Food Chemistry, 153*(15), 353–360.

Li, G., Huang, J., Chen, T., Wang, X., Zhang, H., & Chen, Q. (2017). Insight into the interaction between chitosan and bovine serum albumin insight into the interaction between chitosan and bovine serum albumin. *Carbohydrate Polymers, 176*, 75–82.

Li, H., Zhang, X., Zhao, C., Zhang, H., Chi, Y., Wang, L., … Zhang, X. (2022). Entrapment of curcumin in soy protein isolate using the pH-driven method: Nanoencapsulation and formation mechanism. *LWT- Food Science and Technology, 153*, Article 112480.

Li, J., Du, M., Din, Z. U., Xu, P., Chen, L., Chen, X., … Cai, J. (2023). Multiscale structure characterization of ozone oxidized waxy rice starch. *Carbohydrate Polymers, 307*, Article 120624.

Li, K., Kang, Z. L., Zou, Y. F., Xu, X. L., & Zhou, G. H. (2015). Effect of ultrasound treatment on functional properties of reduced-salt chicken breast meat batter. *Journal of Food Science and Technology, 52*(5), 2622–2633.

Li, Z., Wang, J., Zheng, B., & Guo, Z. (2019). Effects of high pressure processing on gelation properties and molecular forces of myosin containing deacetylated konjac glucomannan. *Food Chemistry, 291*, 117–125.

Liu, C. M., Zhong, J. Z., Liu, W., Tu, Z. C., & Wan, J. (2011). Relationship between functional properties and aggregation changes of whey protein induced by high pressure microfluidization. *Journal of Food Science, 76*(4), 341–347.

Lu, X., Qian, S., Wu, X., Lan, T., & Zhang, H. (2024). Research progress of protein complex systems and their application in food: A review. *International Journal of Biological Macromolecules, 265*, Article 130987.

Niu, F., Su, Y., Liu, Y., Wang, G., & Yang, Y. (2014). Ovalbumin-gum arabic interactions: Effect of pH, temperature, salt, biopolymers ratio and total concentration. *Colloids and Surfaces. B, Biointerfaces, 113*(3), 477–482.

Niu, F., Zhou, J., Niu, D., Wang, C., Liu, Y., Su, Y., & Yang, Y. (2015). Synergistic effects of ovalbumin/gum arabic complexes on the stability of emulsions exposed to environmental stress. *Food Hydrocolloids, 47*, 14–20.

O'Flynn, T. D., Hogan, S. A., Daly, D. F. M., O'Mahony, J. A., & Mccarthy, N. A. (2021). Rheological and solubility properties of soy protein isolate. *Molecules, 26*(10), 3015.

Qin, P., Wang, T., & Luo, Y. (2022). A review on plant-based proteins from soybean: Health benefits and soy product development. *Journal of Agriculture and Food Research, 7*, Article 100265.

Renkema, J., & van Vliet, T. (2002). Heat-induced gel formation by soy proteins at neutral pH. *Journal of Agricultural and Food Chemistry, 50*(6), 1569–1573.

Ru, Q., Wang, Y., Lee, J., Ding, Y., & Huang, Q. (2012). Turbidity and rheological properties of bovine serum albumin/pectin coacervates: Effect of salt concentration and initial protein/polysaccharide ratio. *Carbohydrate Polymers, 88*(3), 838–846.

Saricaoglu, F. T. (2019). Application of high-pressure homogenization (HPH) to modify functional, structural and rheological properties of lentil (*Lens culinaris*) proteins. *International Journal of Biological Macromolecules, 144*, 760–769.

Shi, X., Zou, H., Sun, S., Lu, Z., Zhang, T., Gao, J., & Yu, C. (2019). Application of high-pressure homogenization for improving the physicochemical, functional and rheological properties of myofibrillar protein. *International Journal of Biological Macromolecules, 138*, 425–432.

Thrane, M., Paulsen, P. V., Orcutt, M. W., & Krieger, T. M. (2017). Soy protein: Impacts, production, and applications. *Sustainable protein sources*, 23–45.

Waglay, A., Achouri, A., Karboune, S., Zareifard, M. R., & L'Hocine, L. (2019). Pilot plant extraction of potato proteins and their structural and functional properties. *LWT-Food Science and Technology, 113*, Article 108275.

Wang, W., Li, J., Yan, L., Huang, G., & Dong, Z. (2016). Effect of oxidization and chitosan on the surface activity of soy protein isolate. *Carbohydrate Polymers, 151*, 700–706.

Wang, X., Lee, J., Wang, Y. W., & Huang, Q. (2007). Composition and rheological properties of beta-Lactoglobulin/pectin coacervates: Effects of salt concentration and initial protein/polysaccharide ratio. *Biomacromolecules, 8*(3), 992–997.

Xiong, W., Ren, C., Jin, W., Tian, J., Wang, Y., Shah, B. R., … Li, B. (2016). Ovalbumin-chitosan complex coacervation: Phase behavior, thermodynamic and rheological properties. *Food Hydrocolloids, 61*, 895–902.

Xu, W., Tang, Y., Yang, Y., Wang, G., & Zhou, S. (2020). Establishment of a stable complex formed from whey protein isolate and chitosan and its stability under environmental stresses. *International Journal of Biological Macromolecules, 165*(2), 2823–2833.

Xue, F., Zhu, C., Liu, F., Wang, S., Liu, H., & Li, C. (2018). Effects of high-intensity ultrasound treatment on functional properties of plum (Pruni domesticae semen) seed protein isolate. *Journal of the Ence of Food & Agriculture, 98*, 5690–5699.

Yuan, B., Ren, J., Zhao, M., Luo, D., & Gu, L. (2012). Effects of limited enzymatic hydrolysis with pepsin and high-pressure homogenization on the functional properties of soybean protein isolate. *LWT - Food Science and Technology, 46*(2), 453–459.

Yuan, Y., Wan, Z. L., Yang, X. Q., & Yin, S. W. (2014). Associative interactions between chitosan and soy protein fractions: Effects of pH, mixing ratio, heat treatment and ionic strength. *Food Research International, 55*, 207–214.

Zhang, Q. T., Tu, Z. C., Wang, H., Huang, X. Q., Fan, L. L., Bao, Z. Y., & Xiao, H. (2015). Functional properties and structure changes of soybean protein isolate after subcritical water treatment. *Journal of Food Science and Technology, 52*(6), 3412–3421.

Zhang, X., Liu, Y., Wang, Y., Luo, X., Li, Y., Li, B., … S.. (2019). Surface modification of cellulose nanofibrils with protein nanoparticles for enhancing the stabilization of O/W Pickering emulsions. *Food Hydrocolloids, 97*, Article 105180.

Zhang, X., Zhou, J., Chen, J., Li, B., Li, Y., & Liu, S. (2020). Edible foam based on Pickering effect of bacterial cellulose nanofibrils and soy protein isolates featuring interfacial network stabilization. *Food Hydrocolloids, 100*, Article 105440.

Zheng, L., Regenstein, J. M., Zhou, L., & Wang, Z. (2022). Soy protein isolates: A review of their composition, aggregation, and gelation. *Comprehensive Reviews in Food Science and Food Safety, 21*(2), 1940–1957.